Title
Field implementation of cellulose nanocrystals (CNC) in concrete pavement test track

Journal
International Journal of Pavement Engineering, 25(1)

ISSN
1029-8436

Authors
Haider, Mostofa
Roy, Souvik
Paniagua, Fabian
et al.

Publication Date
2024-12-31

DOI
10.1080/10298436.2024.2375429

Field Implementation of Cellulose Nanocrystals (CNC) in Concrete Pavement Test Track

Authors:

Md Mostofa Haider[a], Souvik Roy[a], Fabian Paniagua[a], Somayeh Nassiri[a*], Angel Mateos[a]

[a]*Department of Civil and Environmental Engineering, University of California Davis, CA 95616*

[*]Phone: 530-752-8918, Email: nassiri@ucdavis.edu

Field Implementation of Cellulose Nanocrystals (CNC) in Concrete Pavement Test Track

This pilot study aimed to fill the knowledge gap on incorporating cellulose nanocrystals (CNC) in concrete pavements in real-world construction settings. The constructability of CNC concrete was evaluated, and the fresh and hardened properties were fully characterized. A series of concrete slabs were placed using ordinary portland cement concrete (OPC mix), portland limestone cement concrete (PLC mix), and PLC-concrete with CNC at a dosage of 0.10% wt. of cementitious materials (CNC mix). CNC and PLC mix showed no significant differences in consistency, workability, and other fresh properties. The addition of CNC did not show significant changes in cumulative heat over PLC. CNC did not lead to notable changes in compressive and flexural strength, modulus of elasticity, coefficient of thermal expansion (CTE), and electrical resistivity. However, the CNC mix had a notably 9% lower drying shrinkage strain at seven months than the PLC mix. The PLC mix exhibited the lowest water absorption rate, while CNC did not induce significant changes. Overall, this study highlights the constructability of concrete slabs with CNC, with notable contributions of CNC to reducing long-term drying shrinkage.

Keywords: Portland Limestone Cement, Cellulose Nanocrystals, Field Constructability, Mechanical properties, Water penetrability.

Nomenclature:

CNC- Cellulose nanocrystals
OPC- Ordinary portland cement
PLC- Portland limestone cement
CTE- Coefficient of thermal expansion
CNF- Cellulose nanofibers
C-S-H Calcium-silicate-hydrate
GGBFS- Granulated blast furnace slag
TEM- Transmission electron microscope
RH- Relative humidity
SSD- Saturated surface-dry
C3S- Tricalcium silicate
C3A- Tricalcium aluminate

1. Introduction

The concrete industry, which relies heavily on portland cement as the primary binding agent of concrete, is under global and regional scrutiny to reduce its contributions to global CO_2 emissions (IEA 2018). For example, California has enacted a law mandating a 40% reduction in cement industry emissions by 2035 to reach zero emissions by 2045 (Becker and Weiner 2021). In this context, it has become necessary to prioritize sustainable objectives without compromising and ideally enhancing the performance and longevity of concrete. In this direction, recent research and implementation efforts have focused on supplementary cementitious materials, novel cements, and innovative additives to replace portland cement or enhance concrete performance (Miller 2018).

Fibers derived from cellulose, the most abundant biopolymer globally, have recently garnered attention in diverse industrial and engineering applications at the micro and nanoscale. In microscale size, cellulose fibers have been shown to enhance various aspects of concrete performance. Particularly, cellulose fibers help mitigate crack development, increase fracture toughness, and reduce plastic shrinkage (Soroushian and Ravanbakhsh 1998, Rapoport and Surendra Shah 2005, Peters *et al.* 2010, Ma *et al.* 2014). Additionally, the emergence of nanotechnology, including cellulose nanomaterials, has prompted significant interest in concrete research due to desirable properties such as large surface area, abundant functional hydroxyl group leading to hydrophilicity and uniform dispersion, and good tensile strength and modulus (Zheng *et al.* 2023). Two morphologically different cellulose nanomaterials have been used in cement applications, i.e., cellulose nanocrystals (CNCs) and cellulose nanofibers (CNFs). CNCs are rod-like in shape and exist as separate individual fibers, while CNFs possess an interconnected network morphology consisting of long nanofibrils with a high aspect ratio (Nassiri *et al.* 2021). CNC is produced by acid hydrolysis to separate the amorphous region from the cellulose structure. CNC has excellent mechanical properties, a high elastic modulus of 150 GPa, a high surface area (9.95×10^5-14.93×10^5 cm^2/g), and a low aspect ratio (10-70) (Zheng *et al.* 2023).

Cellulose nanomaterials have been extensively researched for cementitious composites in recent years. Nonetheless, these are primarily in laboratory evaluation studies that remain at the cement paste or mortar scale and do not advance to the concrete application scale, as reviewed below. These studies have focused on various cement behavior and performance aspects, including rheology, hydration kinetics, and mechanical properties. A literature review is provided on the multiple impacts of cellulose nanomaterials on the properties of cementitious materials.

2. Literature Review

Cellulose nanomaterials exert a substantial impact on the rheological characteristics of cement-based composites. Cao et al. (2015) investigated the influence of CNC dosage obtained by acid hydrolysis on the yield stress of fresh cement paste (Cao *et al.* 2015). The researchers observed a decline in yield stress with increasing CNC dosage up to 0.0206%wt of cement, followed by an increase beyond this concentration. The yield stress reached a level comparable to the control at 0.153%wt CNC and exhibited a considerable increase beyond this threshold. This behavior was attributed to two main mechanisms. The reduction in yield stress at low CNC content is likely due to steric stabilization, similar to the observed mechanism in water-reducing admixtures. Conversely, at higher CNC concentrations, the aggregation of CNC particles forms a network that necessitates more energy to disrupt or align within the cement paste, leading to higher yield stress (Nassiri *et al.* 2021).

Furthermore, Cao et al. (2015) observed retardation of hydration caused by CNC, as evidenced by delayed heat flow during the initial 40 hours of hydration (Cao *et al.* 2015). They attributed this retardation to the adsorption of CNC onto cement particles, impeding their reaction with water during the early stages of hydration. Other researchers have reported similar retardation effects as well (Flores, Kamali, *et al.* 2017, Fu *et al.* 2017, Ghahari *et al.* 2020, Raghunath *et al.* 2023, Wang *et al.* 2023). CNC prolonged the induction period and delayed and decreased the peak heat rate. CNC reduced the contact area between C_3S and water because their adsorption on the C_3S has a large electrostatic effect, thus reducing the hydration heat rate. They found that CNC increased the growth of calcium hydroxide [$Ca(OH)_2$] in the crystal plane, decreased polymerization, and reduced the mean chain length of silicates. CNC provides an additional surface where Ca and Si ions are absorbed, and calcium-silicate-hydrate (C-S-H) gel is formed.

Some studies have shown that the incorporation of nanocellulose into cementitious composites could lead to improvements in mechanical properties. Zubair *et al.* 2022 studied the effect of CNC produced by the acid hydrolysis process from office waste paper and demonstrated the potential of CNC in cement mortar with an improved compressive strength of 37.4 MPa and flexural strength of 5.1 MPa at 0.5% wt of cement. Jiao *et al.* 2016 found that adding 0.15%wt cellulose nanofibers (CNF) to the cement paste resulted in a 15% increase in flexural strength and a 20% increase in compressive strength, which was attributed to enhanced hydration and reduced porosity due to the formation of a denser matrix. Another study reported a 15% to 25% improvement in mechanical properties with CNF doses 0.05%wt and 0.10%wt (Hisseine *et al.* 2019). The researchers proposed that the high-stiffness CNF contributes to the stiffness of high-density C-S-H surrounding anhydrate cement particles, resulting in a higher volume of high-density C-S-H and improved mechanical properties (Hisseine *et al.* 2019). Zhong *et al.* 2022 described four possible mechanisms for improved mechanical properties with polysaccharide nanomaterials, especially CNC and CNF. The four mechanisms are bridging effects, increased modulus due to filler effect with high modulus CNC/CNF, nucleation sites for more cement hydrate to grow, and improved hydrations by internal curing. The latter mechanism is because CNFs can absorb and release water gradually, which could promote the reaction of more anhydrate cement over an extended hydration period, thereby reducing micropores and further enhancing the mechanical properties of the cement paste (Jiao *et al.* 2016). Cao *et al.* 2015 investigated the effect of varying concentrations of CNC on flexural strength. The researchers observed that the flexural strength increased with increasing CNC concentration, reaching a maximum improvement of 30% at 0.102%wt CNC. However, further increases in CNC content led to decreased flexural strength due to CNC agglomeration, which creates weak points for stress concentrations within the cement paste. Another study to note is Zheng *et al.* 2023 study of the mechanism of CNC in cement hydration, particularly on the hydration of C_3S.

There are a few studies on the effect of cellulose nanomaterials in concrete. Hisseine, Omran, *et al.* 2018 examined the impact of CNFs derived from wood pulp on the rheological and mechanical properties of self-consolidating concrete. Notably, significant changes were observed in the fresh properties of the concrete when the CNF content reached a percolation threshold of 0.12%wt. This threshold represents the minimum CNF content required to form a continuous network of interconnected fibrils. The hydrophilic nature of CNFs, attributed to the presence of surface hydroxyl (OH^-) groups, leads to water absorption and contributes to the percolation effect. Moreover, the flexible nature of CNFs plays a vital role in establishing an entangled network, which reduces mobility and hence decreases the workability of the mix (Nassiri *et al.* 2021). Furthermore, higher CNF contents result in increased air entrapment, which can reduce viscosity but have a detrimental impact on compressive strength (Nassiri *et al.* 2021). As viscosity increases, CNF exhibits shear-thinning behavior, aligning the CNF networks in the flow direction and enhancing mixture stability by reducing resistance to flow. Barnat-Hunek *et al.* 2019 investigate the effect of adding CNFs and CNCs on the physical properties of concrete. The researchers found that adding CNFs and CNCs to concrete improved compressive strength, flexural strength, fracture toughness, and reduced water absorption and shrinkage. The study also revealed that the optimal dosage of CNFs and CNCs for enhancing the properties of concrete was 0.1% and 0.5%, respectively. Furthermore, the researchers observed that the addition of CNFs and CNCs did not significantly affect the workability of the concrete mixture. The findings suggest that incorporating CNFs and CNCs into concrete can be a promising approach for enhancing its properties and potential application in the construction industry. Another study used three types of CNC produced from wastepaper by sulfuric acid hydrolysis with varied production parameters at four different doses of 0.25%, 0.5%, 0.75%, and 1% of cement weight (Aziz *et al.* 2021). The study finds that cracking in concrete with CNC is greatly affected by the crystallinity, aspect ratio, and surface roughness of the CNC. CNC with high crystallinity and rougher surface decreased the ultrasonic pulse, which was attributed to the stress concentration that initiated microcracking. For all the CNC, an increase in doses of CNC increased the ultrasonic pulse velocity. The chloride penetrability was reduced with the inclusion of CNC compared to the control without any CNC additives (Aziz *et al.* 2021). The same study finds that the surface hardness of the concrete increased with CNC addition, and higher doses of CNC increased the surface hardness as measured by the Schmidt hammer test. Moreover, CNC with stiff and rougher surfaces resulted in a better surface hardness of the concrete.

3. Knowledge Gaps and scope of this study

Notwithstanding the promising outcomes observed with cellulose nanomaterials in the cement paste and mortar, implementing these nanomaterials at the large concrete construction scale remains rarely evaluated. Challenges include the lack of standards for the nanomaterials, the lack of knowledge and experience on dispersing and incorporating nanomaterials into concrete, specifying the proper dosage for the target concrete application, particularly considering the different morphologies and surface functionalities, and achieving effective dispersion of the material within composite structures, among others. Furthermore, new equipment may be needed to disperse the nanomaterials and add the required amount to the concrete batch (Jamshidi *et al.* 2020). The performance of cellulose nanomaterials relies heavily on their uniform dispersion within the composites. When nanocellulose is applied, hydrogen bonding can form among hydroxyl groups, hindering dispersion (Chu *et al.* 2020). Ultrasonic dispersion is the most used technique to disperse the cellulose nanomaterials in the aqueous media. Most studies reviewed above used laboratory-scale sonication devices to disperse the cellulose nanomaterials in aqueous solutions. However, most ultrasonication devices allow for a few hundred milliliters of solutions at a time. Admixture could be prepared by sonication prior to batching the concrete. However, this will be time-consuming, and it is currently unknown how long the nanomaterials will remain dispersed after ultrasonication. A high shear blending technique was also applied for dispersing cellulose nanomaterials in cement composites (Dhir *et al.* 2007)At present, no accepted standard exists for achieving optimal dispersion of nanomaterials in large-scale concrete production.

Despite extensive laboratory-scale research and promising outcomes for CNC, mostly in the cement paste and mortar industry, there remains a notable shortage of field-scale CNC applications in concrete pavements. Consequently, this study sought to address this gap by conducting a pilot project demonstrating the implementation of CNC in portland limestone cement concrete in conjunction with portland cement, comparing it to conventional Portland cement (OPC) concrete. The evaluation was conducted by constructing a test track of nine slabs at the University of California Pavement Research Facility (UCPRC) in Davis, California.

The primary objective of this study was to provide a comprehensive assessment of the feasibility of employing CNC in concrete pavement and the dispersion method applied. The focus was on constructability and fresh and hardened properties. The tests performed for fresh properties included water content, density, air content, slump, and setting time tests. Hardened properties and durability testing included compressive strength, flexural strength, modulus of elasticity, coefficient of thermal expansion, and drying shrinkage. Bulk electrical resistivity and water absorption tests were performed on the casted and cored specimens to evaluate the durability of the concrete mixes.

4. Materials And Experimental Setup

4.1.Materials

Three sets of concrete slabs were placed, each set using a different concrete mixture. Each set includes three slabs, with one instrumented slab in the middle flanked by two others on each side. The concrete was supplied by a local ready-mix supplier in separate trucks, each with three cubic yard quantities. The three mixtures were concrete with 70% OPC and 30% ground granulated blast furnace slag (GGBFS), concrete with 70%PLC and 30%GGBFS, and concrete with 70%PLC and 30% GGBFS with CNC at a solid dosage of 0.10%wt of cementitious materials. In this paper, these three mixes are referred to as OPC, PLC, and CNC. The chemical compositions and physical properties of the cementitious materials (OPC, PLC, and GGBFS) used in constructing the test track are provided in Table 1.

Table 1. Properties of the Cements and SCMs Used in the Study

Properties	PLC Type IL (15)	OPC Type II/V	GGBFS
Chemical Compositions	%wt.	%wt.	%wt.
Na_2O	0.4	0.7	1.0
MgO	3.9	1.0	12.9
Al_2O_3	3.6	3.5	13.0
SiO_2	15.3	13.3	25.6
P_2O	0.1	0.1	0.0
SO_3	9.7	12.4	7.6
K_2O	0.6	0.6	0.4
CaO	62.7	64.9	37.0
TiO_2	0.1	0.1	0.8
Cr_2O_3	0.0	0.0	0.0
MnO	0.1	0.1	0.8
Fe_2O_3	3.7	3.3	0.8
Physical Properties			
Blaine Fineness (cm^2/g)	5470	4184	4780
Relative Density	3.06	3.15	2.9
Air Content (%)	8.0	6.1	3
Loss on Ignition (LOI) (%)	5.6	2.6	2.1

A breakdown of the proportions and constituents of the three concrete mixtures is presented in Table 2. The amount of water and admixture added was kept the same for all three mixtures. The water in the CNC suspension was subtracted from the total mix water so that all three mixes had the same water content.

Table 2. Ready-mix concrete mixture proportioning (per 1 m3) and the fresh properties of the concrete

Mix Proportioning		
Material	**Description**	**Design Quantity**
Coarse Aggregate	Gravel	1,127 kg (SSD weight)
Fine Aggregate	Sand	1,019 kg (SSD weight)
Cement	Type II/V ordinary portland cement (OPC) or portland limestone cement (PLC) 1L ASTM C150 (ASTM C150-22 2022)	245 kg
GGBFS	Slag, Grade 120, ASTM C989 (ASTM C989-22 2022)	105 kg
Water reducer	Type F: Water Reducing Admixture, High Range (ASTM C494) (ASTM C494-19 2019)	250 g/100 kg of cement
Water	Potable water	34.0 gal

SSD: Saturated surface dry

The CNC used in this study was supplied by the Forest Products Laboratory (FPL) and was produced by sulfuric acid digestion. As stated by FPL, CNC produced through this method possesses sulfuric half-esters on its surface. The CNC was made from bleached wood pulps and had a diameter of 5 nm and a length of 150 nm. The product was provided as a suspension with a CNC solids content of 10.4%. The CNC dose was 0.1% by weight of the total cementitious materials, which amounts to 349 g. of CNC solids per m^3 concrete. According to the literature, the suggested doses of CNC applied in cement composites were between 0.05% and 1.50% of cement weight (Barnat-Hunek *et al.* 2019, Nasir *et al.* 2022). Based on this range, a dosage of 0.10%wt of cementitious materials was tested and confirmed to produce a workable mixture in laboratory trial batches before construction.

Since ultrasonication is only possible on small-size samples at a time, the possibility of using a high-shear blender (Waring CB15 Commercial Blender) at 4000 rpm for dispersion was evaluated. An initial dispersion study was performed to determine the effectiveness of high-shear blending in dispersing CNC in water. CNC was added to the water at 0.1wt% and blended for 10 mins. Transmission electron microscope (TEM) images of the resulting solution were taken at different magnifications to observe the dispersion effectiveness by comparing the image after 10 mins of ultrasonication. One example TEM image of CNCs after ultrasonication and one after shear blending are shown as examples in **Figure 1**b&b, respectively. Many other similar images were compared. Based on observation of the TEM images, it was determined that high shear blending produces similar dispersion effectiveness as ultrasonication and was decided to be used for dispersion of CNC for construction.

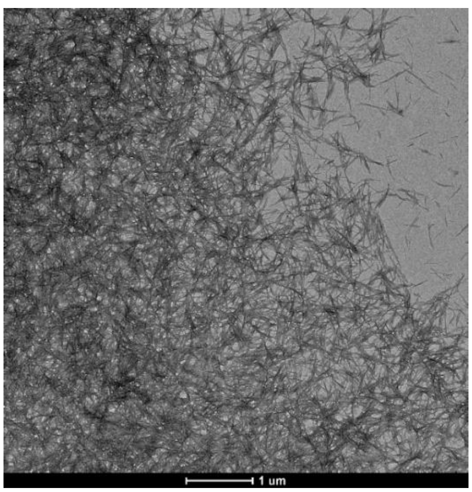

(a)

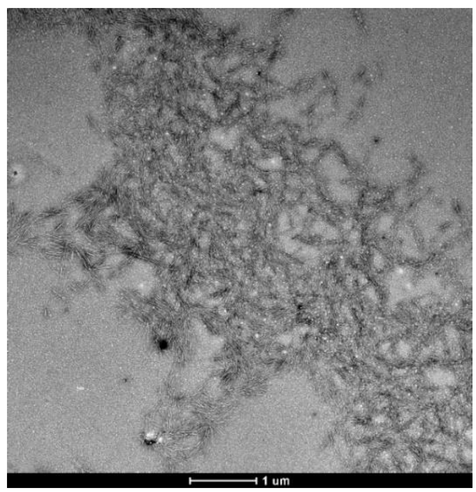

(b)

Figure 1. TEM image of CNC after dispersing in water (a) after 10 mins of ultrasonication (b) after 10 mins of high shear blending

a. CNC Addition

The CNC was dispersed in water by a high-shear blender 4-5 hours before mixing into the concrete. The suspension's CNC solids content was 3.33%. When the concrete truck arrived at the construction site, the CNC suspension was added to the ready-mix truck from the hopper (Figure 2). The concrete was mixed in the truck at the maximum speed (14-16 rpm) for five minutes to incorporate the CNC into the mix.

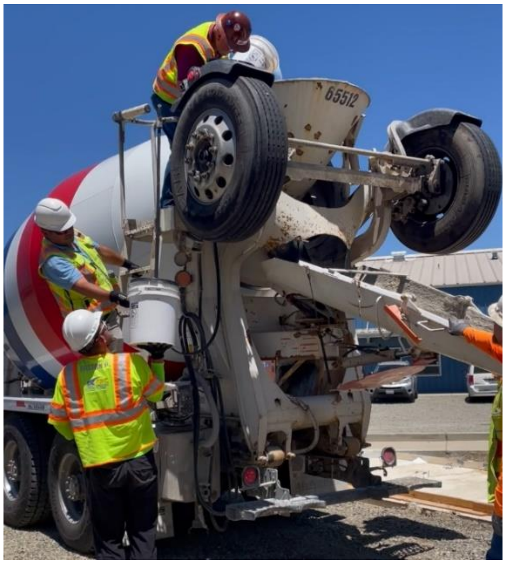

Figure 2. Adding the CNC suspension to the ready-mix truck from the hopper at the construction site

b. Quality Control Tests

Quality control tests were performed on the ready-mix concrete for the test track construction. Table 3 Shows the test results of fresh properties, including water content, density (ASTM C138-23 2023), air content (ASTM C138-23 2023), slump, and setting time (ASTM C403-23 2023) performed on the sieved-out mortar portion. The water content of the fresh concrete was measured following AASHTO T 318 (AASHTO T318-15(2023) 2023) on three samples per mixture type.

Table 3. Fresh properties of the concrete

Fresh Properties of Tested Concrete Mixture			
Property	**OPC**	**PLC**	**CNC**

Slump (mm)	195	165	145
Air Content (%)	1.9	2.20	1.90
Unit Weight (kg/m^3)	88.87	86.97	87.69
Temp (°C)	31.6	31.2	29.7
Initial set time (hr:min)	4:05	3:25	3:45
Final set time (hr: min)	5:25	4:30	4:55

In addition to the construction quality control tests, isothermal calorimetry testing was performed on mortar mixtures prepared with OPC and PLC with two different doses of 0.05% wt. and 0.10% wt. of cementitious materials at 23°C for 7 days. The evolution of heat released with time elapsed was used to determine the impact of CNC on the hydration kinetics of the OPC and PLC mixes.

Concrete specimens were prepared from samples from the corresponding ready-mix truck during test track construction for hardened properties. Following the 24-hour curing period in curing boxes on site, following (ASTM C31-23 2023), the specimens were de-molded and stored in a limewater bath maintained at 23°C until testing. Three specimens were tested for each property at each age. Mechanical performances at 10 days, 28 days, 4 months, and one year age dates were evaluated in terms of compressive strength (ASTM C39-21 2021) using 100 mm × 200 mm (dia. by height) cylinders, flexural strength (ASTM C78/C78M − 22 2022) on 150 mm ×150 mm ×500 mm beams, and modulus of elasticity (ASTM C469-22 2022) on 150 mm ×300 mm (dia. by height) cylinders. The coefficient of thermal expansion (CTE) of each mixture was determined using 100 mm ×175 mm cylinder at 42 days following (AASHTO T336-15(2019) 2019). Drying shrinkage was determined using 100 mm ×100 mm ×275 mm prisms according to (ASTM C157-17 2017).

The performance and durability of concrete under harsh conditions heavily rely on its ability to resist the penetration of water that carries harmful ions through the pore system. Bulk electrical resistivity testing was performed to assess this feature of the mixtures (ASTM C1876-19 2019). In addition, the water adsorption test (ASTM C1585-20 2020) was performed on cores extracted from the slabs approximately 290 days after the test track construction. The initial and secondary absorption rates were calculated based on the slopes of the best-fitted lines for 1 minute to 6 hours and 1 day to 7 days, respectively.

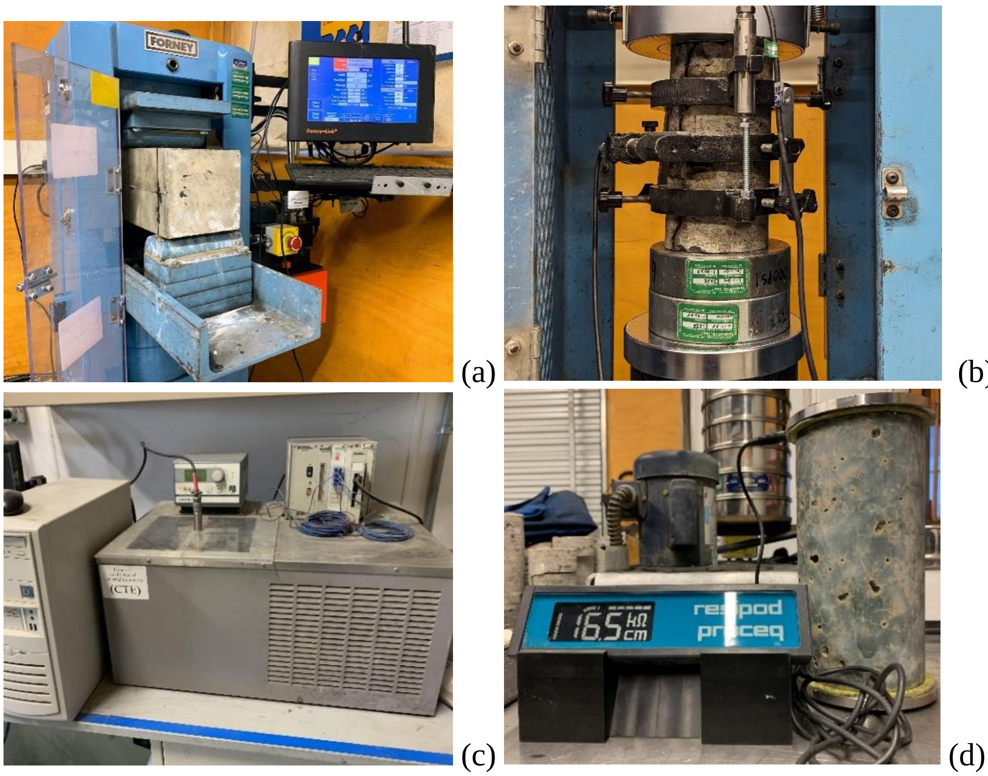

Figure 3. Test setup (a) Flexural strength (b) Modulus of elasticity (c) CTE and (d) Electrical resistivity

5. Design and construction of test sections

a. Test Sections Configuration

The test track is a walking path approximately 13.71 m long. Along this length, three sets of test sections were constructed, each dedicated to a specific type of mixture, as discussed before. These sections consist of three consecutive slabs, each measuring 1.52 m long and 2.44 m wide, as shown in Figure 4a. As shown in Figure 4b, the 100 mm. thick slabs are placed on a 100-mm thick lean concrete base placed on a 75-mm to 100-mm thick aggregate subbase. The subgrade is clay type. The shoulder was backfilled with loose aggregates after the construction of the concrete slabs.

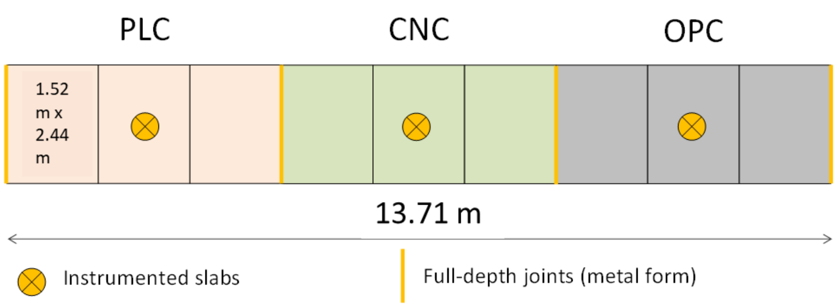

(a)

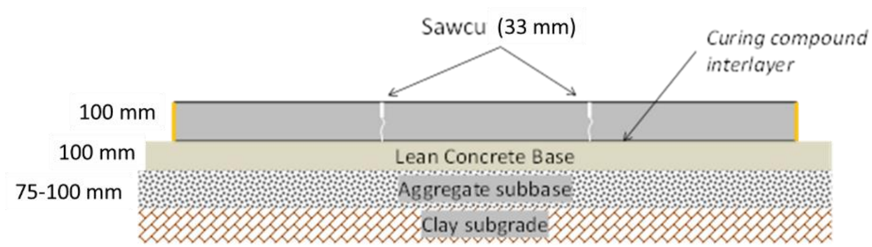

(b)

Figure 4. (a) Test sections layout for three concrete mixes (b) Test sections cross-section

b. Construction of Concrete Slabs

The weather conditions during paving were dry and warm, with maximum air temperature and minimum relative humidity (RH) during the paving hours at approximately 40.5°C and 15%, respectively. The sky was sunny, and the wind speed was below 3.2 kph. Air minimum temperature and maximum RH during the first nights after construction were approximately 60°F and 80%, respectively. Days following construction had similar weather conditions, typical of Davis weather during summer. The concrete was consolidated with a vibrating rolling screed and finished with a trowel. No surface texturing was applied. The curing was conducted with a white-pigmented, resin-based curing compound meeting ASTM C309 Type 2B specifications, applied at a nominal rate of 3.67 m²/l. See pictures of the construction process in **Figure 5**.

Figure 5. Slab construction (a) Rolling screed consolidation of OPC concrete (b) Trowel finishing of PLC section (c) Test sections photograph after few days of casting

6. Results and discussion

a. Fresh Concrete Test Results

The water amount measured in each mixture, an average of three samples per mixture, is summarized in **Figure 6**. The theoretical water content includes the design batch water plus the water absorbed by the aggregates in the saturated surface-dry (SSD) condition. The PLC and the CNC mixtures had similar measured water contents. For the three mixtures, the measured water contents were close to the 9% theoretical water content based on the batch mix design. The measured water contents were 10%, 10.15%, and 9.6%, and the variability among the three tested samples from each mixture is small. The difference between the mix design water and the measured water seems to be within the accuracy of the test method. Sampling errors and aggregate moisture variations might cause the higher values in the measured water content. A study by Robertson and Ley 2020 demonstrated that the use of microwave procedure in

(AASHTO T318-15(2023) 2023) test methods yielded higher w/c ratio than the theoretical w/c ratio with a high coefficient of variation of 8.9%, whereas their proposed test method yielded w/c ratios close to the theoretical w/c ratio.

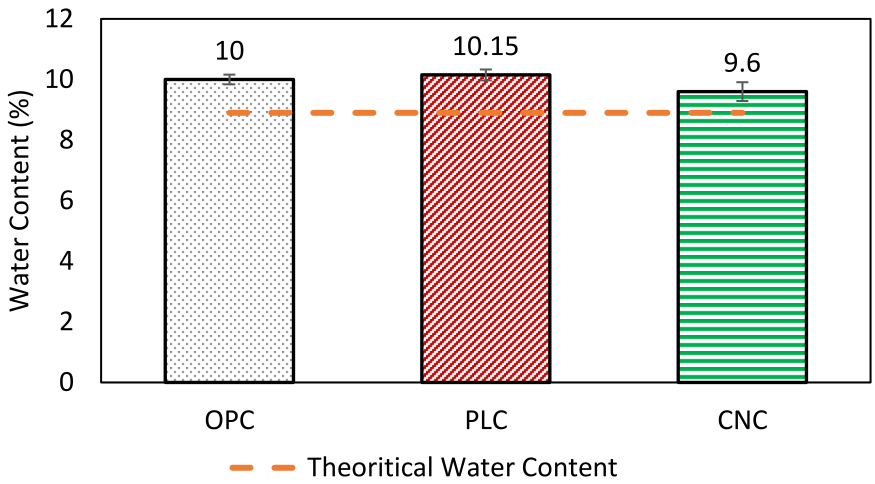

Figure 6. Measured water content (evaporable water / dry weight of mixture, AASHTO T 318)

Fresh concrete test results are presented in **Table 2**Error! Reference source not found.. It is observed that the slump measured for the PLC and CNC mixtures was slightly lower than the OPC mixture. OPC had a higher slump than PLC (195 mm versus 165 mm.), even though the two mixtures had the same measured water content and HRWR admixture. This outcome suggests a higher water demand for PLC versus OPC for the same consistency. This variation in water demand is likely due to the enhanced fineness of the PLC, with Blaine fineness of 5470 cm^2/g compared to OPC Blaine fineness of 4184 cm^2/g. Notably, prior studies have also reported a reduction in slump values when employing PLC, ascribed to the increased specific surface area of PLC (Tsivilis *et al.* 2003). CNC further reduced the slump of the fresh concrete compared to PLC because it is hydrophilic and, due to the presence of hydroxyl groups, could adsorb some of the water from the mix and reduce the slump of concrete (Gómez Hoyos *et al.* 2013)

The other fresh concrete properties (air content and unit weight) were similar for the OPC and CNC mix. The small temperature differences between mixtures are most likely due to the different times of the day when each mixture was placed (CNC at approximately 1:00 pm, PLC at approximately 2:00 pm, and finally, OPC at approximately 3:00 pm).

The initial and final setting times of the OPC were more prolonged compared to the setting times of the PLC and CNC mixtures. Based on penetrating resistance, the initial and final setting times of OPC were 4:05 hr:min and 5:25 hr:min, respectively. The setting times of PLC were approximately 15% shorter (3:25 and 4:30 hr:min for the initial and final set, respectively). The temperature in the middle of each sample was recorded during the setting time experiment. The temperature was slightly, up to 1.1°C, higher inside PLC than OPC due to the higher fineness of PLC. Furthermore, the inclusion of CNC in the mixture resulted in a 20 and 25-minute delay in initial and final setting time, respectively, compared to PLC without CNC. Previous studies have demonstrated that CNC delays the cement's setting time, most likely through the electrostatic dispersion mechanism (Nassiri *et al.* 2021).

The cumulative heat of hydration and heat flow curves from the isothermal calorimetry test are presented in **Figure 7**a-c. In general, the heat flow curve of portland cement shows five different stages of hydration, i.e., the initial reaction period, induction period, acceleration period, deceleration period, and slow reaction stage. The rapid dissolution of cement causes the initial reaction period, hydrolysis reaction of C_3A, and ettringite formation (Chen and Yang 2017). The next stage is the induction period when the reaction, hence the heat release, becomes slow. The induction period is followed by the acceleration period, when mainly the dissolution and reaction of C_3S starts and accelerates the heat flow rate.

Based on **Figure 7**a, shown for the shorter period in **Figure 7**b, the heat flow reaches a maximum (main C_3S peak) at around 8.6 hours for the OPC mix, and then the reaction rate decelerates after about 1 day and becomes flat. A second peak was observed for PLC and CNC after the main C_3S peak, which is smaller in OPC. This additional peak is attributed to the sulfate depletion peak, where C_3A reacts with monosulfate or monocarbonate (Lura *et al.* 2010). Carbonate ions from the limestone in the monocarboaluminate hydrates and sulfate ions in the system result in further ettringite formation (Tydlitát *et al.* 2014)The additional peak was also present on CNC's heat flow curve. However, this peak was not observable for OPC because it was superimposed with the main hydration peak.

A few characteristic parameters as mentioned by (Chen and Yang 2017), i.e., time to onset of C_3S hydration t_1, time to maximum heat flow rate t_2, delay in onset of C_3S hydration t_3, delay to the maximum heat rate t_4 and change in the maximum heat rate, *w(%)* were calculated from the heat rate curve. The t_1 for PLC was reduced to 2.47 hours compared to the 3.70 hours of the OPC, which can be attributed to the carbosilicate hydration in the PLC mix during the dormant period (Tydlitát *et al.* 2014). Also, the higher fineness of PLC compared to OPC may contribute to accelerated hydration. Adding 0.05wt% CNC increased the t_1 by 17 mins compared to the PLC mix. However, for 0.1 wt% CNC, t_1 was similar to the PLC mix. Time to maximum heat rate, $t_{2,}$ was reduced for PLC compared to OPC. However, the addition of CNC delayed the maximum heat rate, $t_{2,}$ compared to both OPC and PLC. The initial acceleration of the hydration with PLC can be attributed to the high Blaine fineness of the PLC, which results in more nucleation sites that promote early-age hydration of C_3S. However, the other hydration reaction remains limited (Moon *et al.* 2017). For the CNC mix, a delay in the peak heat rate compared to the PLC mix was also evident in the setting time tests and is attributed to the dispersion of cement particles by the electrostatic mechanism, as explained by Nassiri et al. (2021) (Nassiri *et al.* 2021). Cellulose nanoparticles have high negative zeta potentials. Nassiri et al. (2021) reported values of -50.6±1.5 mV (at pH = 5.6) and -47.5±2.3 mV (at pH = 7.4) for CNF and CNC respectively (Nassiri *et al.* 2021). Cellulose nanoparticles can be absorbed on positively charged cement grains, particularly C_3A, thereby generating repulsive electrostatic forces and helping disperse cement, which can also delay cement hydration.

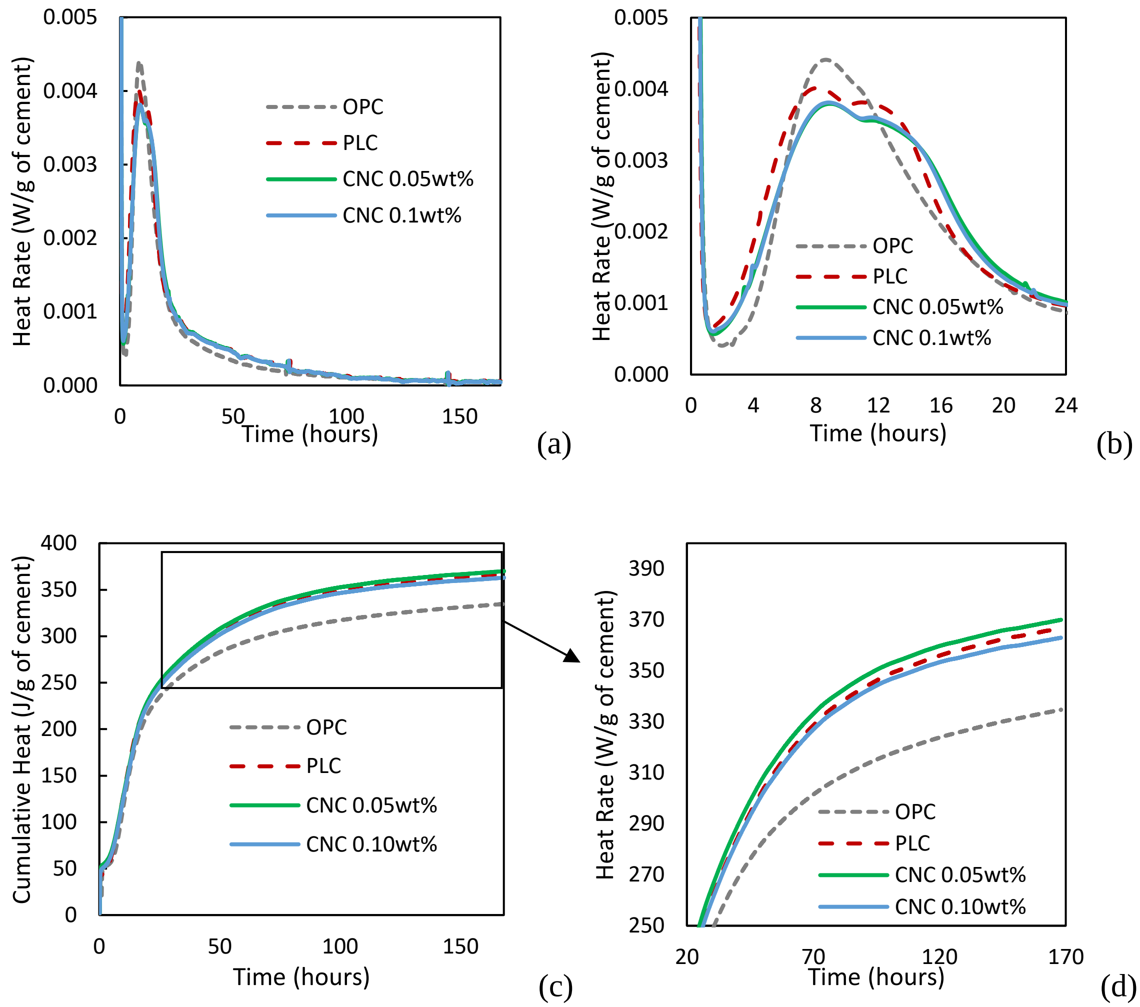

Figure 7. (a) Heat flow rate of the different mixtures up to 7 days (b) Heat rate of the different mixtures up to 24 hrs (c) Cumulative heat of hydrations (d) Zoomed graphs showing the cumulative heat differences at later days

The cumulative heat of the three mixes for 7 days is shown in Figure 7c. The cumulative heat for PLC was 9.55% higher than the OPC after 7 days. After 7 days, the highest cumulative heat was observed for 0.05wt% CNC, which was 10.45% higher than the OPC and 0.82% higher than the PLC. However, 0.1wt% CNC reduced the cumulative heat compared to the PLC by 1.1%.

From the isothermal calorimetry analysis, it can be inferred that adding CNC does not significantly influence the cumulative heat of hydration. Previous studies reported conflicting results in the heat of hydrations with CNC. Cao et al. (2015) reported a 16% increase in cumulative heat after 200 hrs of hydration with 0.8%wt CNC, which they attributed to short circuit diffusion. However, Zheng et al. 2023 reported a maximum 22% and 18% decrease in heat rate and cumulative heat, respectively, with different doses of CNC (0.05 wt% to 0.5 wt%) (Zheng et al. 2023). They assert that the length of CNC is insufficient to cover the surface of cement particles, which may hinder the effectiveness of short-circuit diffusion. It was observed that the peak heat release rate was reduced by including both doses of CNC. Both the study by Cao et al. 2015 and Zheng et al. 2023 reported a decrease in heat release rate with CNC attributed to the reduction of contact area between cement particles and water, which was caused by adhering the CNC to the cement grains due to the strong electrostatic effect of CNC because of its strong hydrophilicity (Cao et al. 2015, Zheng et al. 2023).

b. Hardened Properties

The mechanical performance, i.e., compressive strength, flexural strength, and modulus of elasticity of the three mixes, are shown in Figure 8a-c. Overall, the two mixtures with PLC (CNC and PLC) were similar to each other for all mechanical properties (strength, modulus of elasticity), with differences being either approximately 10% or less (flexural and compressive strength). On the other hand, the CNC and PLC mixtures had approximately 10 to 15% higher strength than the OPC mixture. The higher strength with PLC compared to the OPC was observed by another study (Voglis *et al.* 2005), which was attributed to the filler effect due to fine particles of the limestone and a higher rate of pozzolanic reactivity. Apart from the filler effect, the reaction of C_3A with the $CaCO_3$ of the limestone produces calcium carboaluminates (Bonavetti *et al.* 2001). Moreover, calcium carbosilicate hydrates can be formed in the hydration of C_3S with $CaCO_3$ from limestone (Péra *et al.* 1999). Hence, these mechanisms' filler effect and additional hydrations of C_3A and C_3S in the presence of $CaCO_3$ from limestone, results in the strength improvement of PLC over OPC. The addition of CNC to the PLC did not show any significant improvement in terms of mechanical performance. The statistical paired t-test shows no significant difference in compressive strength, flexural strength, and modulus strength between PLC and CNC at 10d, 28d, and 120d at 95% confidence level with all p-value higher than 0.05, except 120d flexural strength where CNC showed a significant 6% decrease in flexural strength over PLC (p-value 0.024). However, previous studies showed improvement in compressive and flexural strength with CNC, mostly in cement paste and mortar (Cao *et al.* 2015, Barnat-Hunek *et al.* 2019, Nassiri *et al.* 2021).

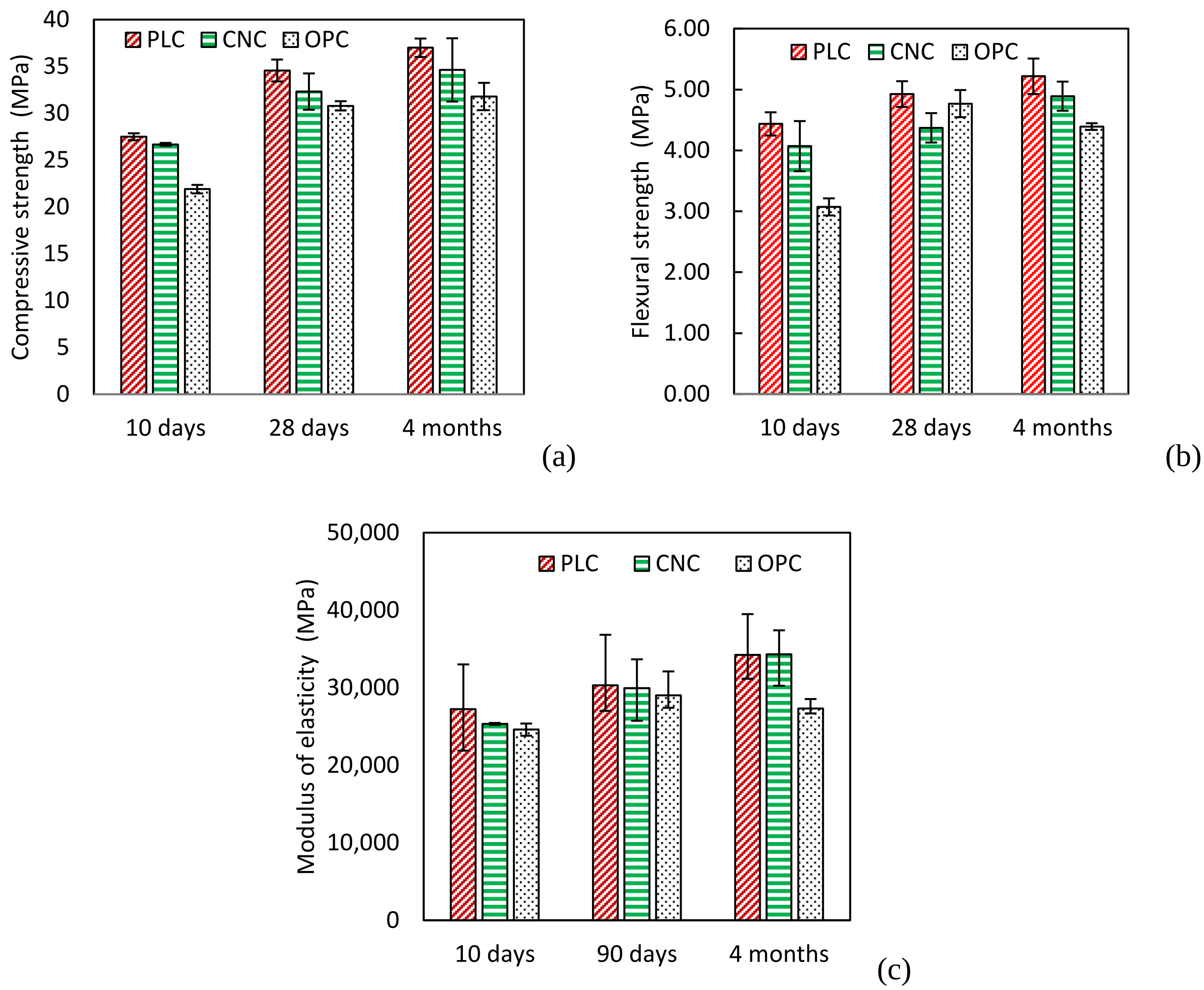

Figure 8. (a) Compressive strength, (b) Flexural strength, and (c) Modulus of elasticity of the different mixtures

c. Thermal Property and Drying Shrinkage

The CTE and drying shrinkage of the three mixes are shown in Figure 10a-b. The PLC mixture presented a higher CTE of 10.04 με/°C compared to the 9.37 με/°C of OPC and 9.86 με/°C CTE of CNC. The difference in CTE of PLC and OPC is approximately 7%. Malakopoulos et al. 2021 reported a 30% decrease in CTE with limestone cement compared to the OPC (Malakopoulos *et al.* 2021).

Regarding drying shrinkage, PLC resulted in higher strains in the short term (6 days drying) but lower strains at 4 and 7 months, compared to OPC. At 4 and 7 months, the differences between the two mixtures with PLC versus OPC were statistically significant. Malakopoulos et al. 2021 reported a decrease in drying shrinkage with PLC compared to the OPC, which they attributed to the higher alkali content of OPC, as higher alkali content was found to increase the drying shrinkage (Malakopoulos *et al.* 2021). CNC showed the lowest drying shrinkage compared to PLC and OPC at all times. CNC was 9% lower in drying shrinkage strain at seven months of age than PLC. CNC's ability to retain water can assist in minimizing drying shrinkage. Other studies reported reductions in autogenous shrinkage by CNF by 36% due to the increased degree of hydration (Hisseine, Basic, *et al.* 2018). The reduction in long-term drying shrinkage could be from the different ways CNCs may influence C-S-H. For example, it was interpreted that with CNC, more high-density C-S-H was produced (Flores, Mahsa Kamali, *et al.* 2017). Others also suggested that CNC resulted in more high-density C-S-H and higher flexural capacity (Cao *et al.* 2015). These changes in the stiffness and microstructure of the C-S-H could be the reason for changes seen in drying shrinkage; however, more testing of C-S-H and other hydrate phases is required to fundamentally understand the impact of CNC on drying shrinkage.

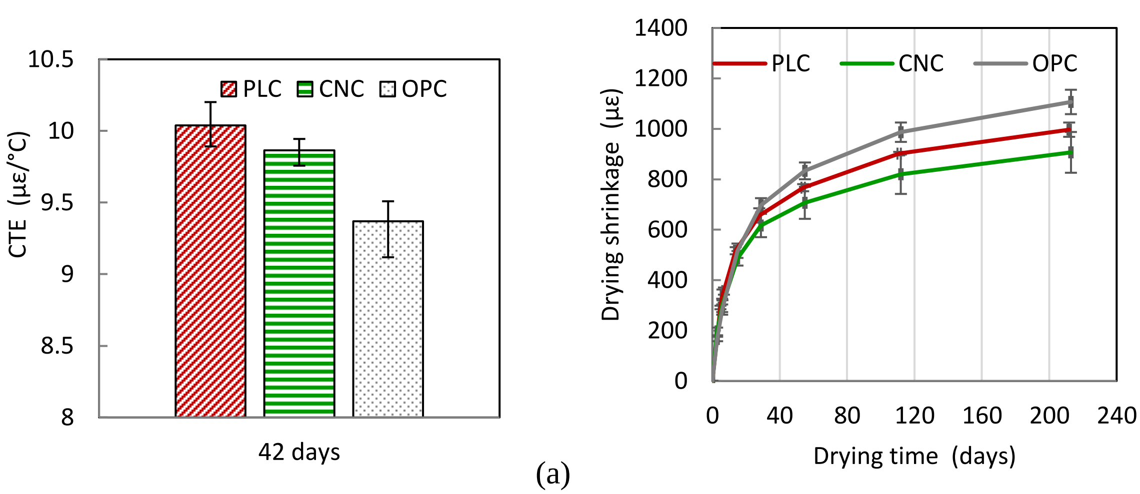

(a) (b)

Figure 9. (a) CTE and (b) Drying shrinkage of the different mixtures.

d. Durability

The bulk electrical resistivity of all three mixtures is shown in Figure 10. The PLC and CNC mixtures had considerably better (higher) resistivity than the OPC ones. The increased electrical resistivity indicates a more refined pore structure and a less interconnected pore system to convey the ions (Lollini et al. 2014). Lollini et al. 2014 reported an early age increase in electrical resistivity at 1 day for PLC compared to OPC, which was decreased later from 7 days and reported a reduction of 36% in electrical resistivity at 360 days (Lollini et al. 2014). Nevertheless, a consistently higher resistivity for PLC mixtures is seen compared to OPC at all ages. The electrical resistivity measures the impedance to the movement of ions under an applied electrical field, hence an indicator of the transport properties of the concrete. Pore size, pore connectivity, and pore volume are important factors that influence the bulk resistivity of concrete. Increased resistivity suggests the discontinuity of the pore system (Azarsa and Gupta 2017). PLC and CNC, due to their higher degree of reactivity and filler effect, may fill more pore spaces and reduce the pore sizes, thus reducing the pore connectivity, which eventually increases the electrical resistivity compared to the OPC mix.

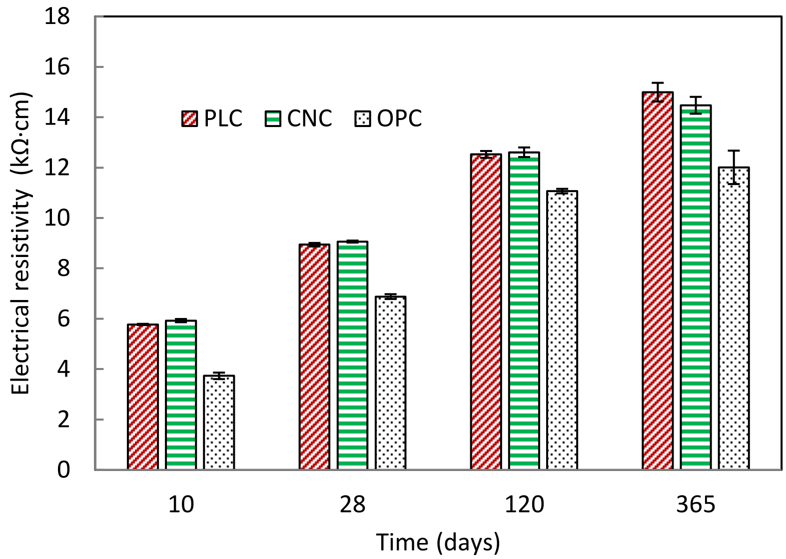

Figure 10. Bulk electrical resistivity results for all mixtures

Water absorption tests were performed on the cored samples extracted from the test track. The average absorption curves of two samples of each mix were plotted against the square root of time and shown in Figure 11 (a). The primary and secondary rate of absorption was calculated from the slope of early (up to 6 hours) and later days (1 to 7 days) of the absorptions curve and shown in Figure 11 (b). The water absorption of the OPC was highest among the three mixes. The PLC showed the least absorption during the nine days of the tests, followed by CNC. PLC showed the lowest initial and final rate of absorption. PLC's initial and secondary absorption rates were 1.17 mm/√s and 0.64 mm/√s, respectively, 39% and 63% less than the OPC mix. However, the CNC mix showed a higher initial and secondary rate (1.63 mm/√s and 0.89 mm/√s, respectively) of water absorption than the PLC mix. PLC has finer particle sizes, acts as a filler, and refines the concrete microstructure to reduce water absorption and improve durability (Dhir *et al.* 2007). The decrease in water permeability with PLC was reported in previous studies (Tsivilis *et al.* 2003, Dhir *et al.* 2007, Chen *et al.* 2014). Tsivilis et al. (2003) reported decreased water permeability and sorption of PLC concrete compared to OPC concrete (Tsivilis *et al.* 2003). However, the same study noticed an increase in gas permeability with PLC. The permeability of concrete is not solely determined by its porosity; it also depends on factors such as pore size, distribution, shape, tortuosity, and pore connectivity (Tsivilis *et al.* 2003) The author concluded that gas permeability is mainly linked to porosity, and water absorption is governed by pore types and sizes. The Addition of CNC to PLC did not provide any positive benefits to water absorption compared to the PLC mixture. It has been noticed that the variability of absorption rate with CNC is much higher than that of PLC specimens. Previous research has indicated that concrete reinforced with CNC and CNF exhibits improved resistance against penetrability (Barnat-Hunek *et al.* 2019, Nasir *et al.* 2022). Despite some evidence of decreased water absorption with CNC, the specimens were stored in lab conditions (Barnat-Hunek *et al.* 2019). Hunek et al. (2019) reported a 32% decrease in the water absorption coefficient by adding the 1.5 %vol CNC (Barnat-Hunek *et al.* 2019). The higher water absorption of the CNC samples may result from the construction and other environmental variables in the field conditions.

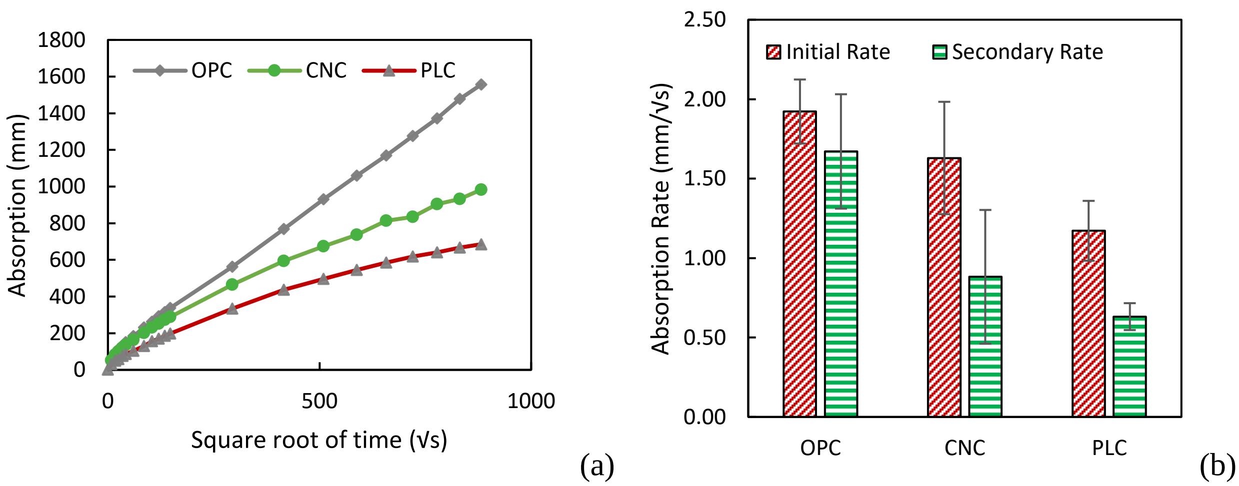

Figure 11. (a) Absorption curve (b) Primary and secondary absorption rate of the tested mixtures.

7. Conclusions

This study evaluated the constructability of concrete pavement slabs with CNC by a nine-slab walk path construction. The key findings of the study are as follows;

- Fresh concrete properties such as slump, air content, and unit weight were the same between CNC and the reference PLC mixtures. The slump value of OPC was slightly higher than that of the PLC.
- The initial and final setting times of the PLC mix were 40 and 55 minutes shorter than those of the OPC mix, respectively, whereas CNC delayed them by 20 and 25 minutes. CNC 0.05wt.% had the highest 7-day cumulative heat of hydration (372.1 J/g) compared to OPC (334.9 J/g) and PLC (367.5 J/g). The heat flow rate of the PLC mix was accelerated by 36 minutes compared to the CNC and OPC mix.
- Hardened properties, including strength, modulus of elasticity, and coefficient of thermal expansion (CTE), were similar based on laboratory tests of specimens cast during construction. Differences observed for flexural and compressive strength were approximately 10% or less. Addition of CNC reduced the CTE of PLC mix by 1.8%. For modulus of elasticity the difference between CNC and PLC mixtures was statistically insignificant at 5% significance.
- At a 7-month concrete age, CNC reduced the drying shrinkage of PLC by 9%. PLC alone reduced the drying shrinkage by 10% relative to the OPC.
- Regarding durability, electrical resistivity increased by 25% with PLC and CNC over the OPC mix at 365 days. Electrical resistivity was the same for PLC and CNC during the study period. The water absorption test demonstrated that the PLC mix had the lowest

absorption rate. The addition of CNC did not affect the water absorption, hence the porosity of the mix.

Based on these findings, it can be concluded that the addition of CNC was implementable at the concrete scale and in full construction settings without any practical or technical challenges. CNC addition did not negatively impact the constructability of the pavement or the fresh concrete properties. The most notable impact of CNC addition was reducing the long-term (7-month) drying shrinkage by 9% for the PLC mix. This effect could have significant positive outcomes regarding drying shrinkage control in dry climates and warrants more investigation in the future. Though significant improvements in mechanical properties were not seen in this study, earlier than 7 days, mechanical properties may be increased by CNC, but those were not tested in this study.

Recommendation and Future Work

- Shear-blending can be a viable option for dispersing CNC in water for large-scale construction.
- The hygrothermal performance will be analyzed for the three instrumented slabs with the three different mixes.
- The early-age properties of CNC concrete require more attention in the future.
- We recommend assessing the performance of CNC for shrinkage control in field conditions accompanied by environmental and traffic loadings.
- LCA and LCCAs are required for the environmental and economic viability for using CNC in the pavement with a full-lifecycle perspective.

- Long-term performance and durability of the concrete pavement with CNC over the life cycle may be assessed in the future.

8. Acknowledgments

The study was performed as part of a sub-award contract with Organ State University's award by the Joint Institute for Wood Product Innovation—contributions of Drs. Jason Wiess and Burkan Isgor, during the concentration and dispersion study and obtaining the CNC sample and trial batches of CNC concrete, are greatly acknowledged. Cemex, and Mr. Mark Hill in particular, for supplying ready-mix concrete for the test track, cooperation with the research team, and facilitating the specific requirements of the research project are greatly acknowledged. Forest Product Laboratory is thanked for supplying cellulose nanocrystals (CNC). The UCPRC staff and students, including Jeffrey Buscheck, Julio Paniagua, Mauricio Melgar, Michael Bowman, and Madelin Barry, are acknowledged for their work on the test track construction.

9. References

AASHTO T318-15(2023), 2023. Standard Method of Test for Water Content of Freshly Mixed Concrete Using Microwave Oven Drying.

AASHTO T336-15(2019), 2019. Standard Method of Test for Coefficient of Thermal Expansion of Hydraulic Cement Concrete.

ASTM C31-23, 2023. Standard Practice for Making and Curing Concrete Test Specimens in the Field.

ASTM C39-21, 2021. Standard Test Method for Compressive Strength of Cylindrical Concrete Specimens.

ASTM C78/C78M − 22, 2022. Standard Test Method for Flexural Strength of Concrete (Using Simple Beam with Third-Point Loading).

ASTM C138-23, 2023. Test Method for Density (Unit Weight), Yield, and Air Content (Gravimetric) of Concrete.

ASTM C150-22, 2022. Standard Specification for Portland Cement.

ASTM C157-17, 2017. Standard Test Method for Length Change of Hardened Hydraulic-Cement Mortar and Concrete.

ASTM C403-23, 2023. Standard Test Method for Time of Setting of Concrete Mixtures by Penetration Resistance.
ASTM C469-22, 2022. Standard Test Method for Static Modulus of Elasticity and Poisson's Ratio of Concrete in Compression.
ASTM C494-19, 2019. Standard Specification for Chemical Admixtures for Concrete.
ASTM C989-22, 2022. Specification for Slag Cement for Use in Concrete and Mortars.
ASTM C1585-20, 2020. Standard Test Method for Measurement of Rate of Absorption of Water by Hydraulic-Cement Concretes.
ASTM C1876-19, 2019. Standard Test Method for Bulk Electrical Resistivity or Bulk Conductivity of Concrete.
Azarsa, P. and Gupta, R., 2017. Electrical Resistivity of Concrete for Durability Evaluation: A Review. *Advances in Materials Science and Engineering*, 2017, 1–30.
Aziz, M.A., Zubair, M., and Saleem, M., 2021. Development and testing of cellulose nanocrystal-based concrete. *Case Studies in Construction Materials*, 15, e00761.
Barnat-Hunek, D., Grzegorczyk-Frańczak, M., Szymańska-Chargot, M., and Łagód, G., 2019. Effect of Eco-Friendly Cellulose Nanocrystals on Physical Properties of Cement Mortars. *Polymers*, 11 (12), 2088.
Becker and Weiner, 2021. Bill Status - SB-596 Greenhouse gases: cement sector: net-zero emissions strategy [online]. Available from: https://leginfo.legislature.ca.gov/faces/billStatusClient.xhtml?bill_id=202120220SB596 [Accessed 27 Nov 2023].
Bonavetti, V.L., Rahhal, V.F., and Irassar, E.F., 2001. Studies on the carboaluminate formation in limestone filler-blended cements. *Cement and Concrete Research*, 31 (6), 853–859.
Cao, Y., Zavaterri, P., Youngblood, J., Moon, R., and Weiss, J., 2015. The influence of cellulose nanocrystal additions on the performance of cement paste. *Cement and Concrete Composites*, 56, 73–83.
Chen, J.J., Kwan, A.K.H., and Jiang, Y., 2014. Adding limestone fines as cement paste replacement to reduce water permeability and sorptivity of concrete. *Construction and Building Materials*, 56, 87–93.
Chen, Z. and Yang, E.-H., 2017. Early age hydration of blended cement with different size fractions of municipal solid waste incineration bottom ash. *Construction and Building Materials*, 156, 880–890.
Chu, Y., Sun, Y., Wu, W., and Xiao, H., 2020. Dispersion Properties of Nanocellulose: A Review. *Carbohydrate Polymers*, 250, 116892.
Dhir, R.K., Limbachiya, M.C., McCarthy, M.J., and Chaipanich, A., 2007. Evaluation of Portland limestone cements for use in concrete construction. *Materials and Structures*, 40 (5), 459–473.
Flores, J., Kamali, M., and Ghahremaninezhad, A., 2017. An Investigation into the Properties and Microstructure of Cement Mixtures Modified with Cellulose Nanocrystal. *Materials*, 10 (5), 498.
Flores, Mahsa Kamali, and Ali Ghahremaninezhad, 2017. An Investigation into the Properties and Microstructure of Cement Mixtures Modified with Cellulose Nanocrystal. *Materials*, 10 (5), 498.
Fu, T., Montes, F., Suraneni, P., Youngblood, J., and Weiss, J., 2017. The Influence of Cellulose Nanocrystals on the Hydration and Flexural Strength of Portland Cement Pastes. *Polymers*, 9 (12), 424.

Ghahari, S., Assi, L.N., Alsalman, A., and Alyamaç, K.E., 2020. Fracture Properties Evaluation of Cellulose Nanocrystals Cement Paste. *Materials*, 13 (11), 2507.

Gómez Hoyos, C., Cristia, E., and Vázquez, A., 2013. Effect of cellulose microcrystalline particles on properties of cement based composites. *Materials & Design*, 51, 810–818.

Hisseine, O.A., Basic, N., Omran, A.F., and Tagnit-Hamou, A., 2018. Feasibility of using cellulose filaments as a viscosity modifying agent in self-consolidating concrete. *Cement and Concrete Composites*, 94, 327–340.

Hisseine, O.A., Omran, A.F., and Tagnit-Hamou, A., 2018. Influence of Cellulose Filaments on Cement Paste and Concrete. *Journal of Materials in Civil Engineering*, 30 (6), 04018109.

Hisseine, O.A., Wilson, W., Sorelli, L., Tolnai, B., and Tagnit-Hamou, A., 2019. Nanocellulose for improved concrete performance: A macro-to-micro investigation for disclosing the effects of cellulose filaments on strength of cement systems. *Construction and Building Materials*, 206, 84–96.

IEA, 2018. *Technology Roadmap - Low-Carbon Transition in the Cement Industry*.

Jamshidi, A., Kurumisawa, K., White, G., Jize, M., and Nawa, T., 2020. Use of nanotechnology in concrete pavements. *In*: *Smart Nanoconcretes and Cement-Based Materials*. Elsevier, 383–401.

Jiao, L., Su, M., Chen, L., Wang, Y., Zhu, H., and Dai, H., 2016. Natural Cellulose Nanofibers As Sustainable Enhancers in Construction Cement. *PLOS ONE*, 11 (12), e0168422.

Lollini, F., Redaelli, E., and Bertolini, L., 2014. Effects of portland cement replacement with limestone on the properties of hardened concrete. *Cement and Concrete Composites*, 46, 32–40.

Lura, P., Winnefeld, F., and Klemm, S., 2010. Simultaneous measurements of heat of hydration and chemical shrinkage on hardening cement pastes. *Journal of Thermal Analysis and Calorimetry*, 101 (3), 925–932.

Ma, H., Qian, S., and Zhang, Z., 2014. Effect of self-healing on water permeability and mechanical property of Medium-Early-Strength Engineered Cementitious Composites. *Construction and Building Materials*, 68, 92–101.

Malakopoulos, A., Chatzigeorgiou, M., Boukos, N., and Salifoglou, A., 2021. Durability performance of Portland limestone cement mortar containing butyl and zinc stearate admixtures. *Materials and Structures*, 54 (2), 60.

Miller, S.A., 2018. Supplementary cementitious materials to mitigate greenhouse gas emissions from concrete: can there be too much of a good thing? *Journal of Cleaner Production*, 178, 587–598.

Moon, G.D., Oh, S., Jung, S.H., and Choi, Y.C., 2017. Effects of the fineness of limestone powder and cement on the hydration and strength development of PLC concrete. *Construction and Building Materials*, 135, 129–136.

Nasir, M., Aziz, M.A., Zubair, M., Ashraf, N., Hussein, T.N., Allubli, M.K., Manzar, M.S., Al-Kutti, W., and A. Al-Harthi, M., 2022. Engineered cellulose nanocrystals-based cement mortar from office paper waste: Flow, strength, microstructure, and thermal properties. *Journal of Building Engineering*, 51, 104345.

Nassiri, S., Chen, Z., Jian, G., Zhong, T., Haider, M.M., Li, H., Fernandez, C., Sinclair, M., Varga, T., Fifield, L.S., and Wolcott, M., 2021. Comparison of unique effects of two contrasting types of cellulose nanomaterials on setting time, rheology, and compressive strength of cement paste. *Cement and Concrete Composites*, 123, 104201.

Péra, J., Husson, S., and Guilhot, B., 1999. Influence of finely ground limestone on cement hydration. *Cement and Concrete Composites*, 21 (2), 99–105.

Peters, S.J., Rushing, T.S., Landis, E.N., and Cummins, T.K., 2010. Nanocellulose and Microcellulose Fibers for Concrete. *Transportation Research Record: Journal of the Transportation Research Board*, 2142 (1), 25–28.

Raghunath, S., Hoque, M., and Foster, E.J., 2023. On the Roles of Cellulose Nanocrystals in Fiber Cement: Implications for Rheology, Hydration Kinetics, and Mechanical Properties. *ACS Sustainable Chemistry & Engineering*, 11 (29), 10727–10736.

Rapoport, J. and Surendra Shah, 2005. Cast-in-Place Cellulose Fiber-Reinforced Cement Paste, Mortar, and Concrete. *ACI Materials Journal*, 102 (5).

Robertson, J.B. and Ley, M.T., 2020. Determining the water to cement ratio of fresh concrete by evaporation. *Construction and Building Materials*, 242, 117972.

Soroushian, P. and Ravanbakhsh, S., 1998. Control of Plastic Shrinkage Cracking with Specialty Cellulose Fibers. *ACI Materials Journal*, 95 (4).

Tsivilis, S., Tsantilas, J., Kakali, G., Chaniotakis, E., and Sakellariou, A., 2003. The permeability of Portland limestone cement concrete. *Cement and Concrete Research*, 33 (9), 1465–1471.

Tydlitát, V., Matas, T., and Černý, R., 2014. Effect of w/c and temperature on the early-stage hydration heat development in Portland-limestone cement. *Construction and Building Materials*, 50, 140–147.

Voglis, N., Kakali, G., Chaniotakis, E., and Tsivilis, S., 2005. Portland-limestone cements. Their properties and hydration compared to those of other composite cements. *Cement and Concrete Composites*, 27 (2), 191–196.

Wang, Y., Goodman, S., Bao, Y., and Meng, W., 2023. Morphological, microstructural, and mechanical properties of highly-ordered C–S–H regulated by cellulose nanocrystals (CNCs). *Cement and Concrete Composites*, 143, 105276.

Zheng, D., Yang, H., Feng, W., Fang, Y., and Cui, H., 2023. Modification mechanism of cellulose nanocrystals in cement. *Cement and Concrete Research*, 165, 107089.

Zhong, T., Jian, G., Chen, Z., Wolcott, M., Nassiri, S., and Fernandez, C.A., 2022. Interfacial interactions and reinforcing mechanisms of cellulose and chitin nanomaterials and starch derivatives for cement and concrete strength and durability enhancement: A review. *Nanotechnology Reviews*, 11 (1), 2673–2713.

Zubair, M., Mu'azu, N.D., Nasir, M., Manzar, M.S., Aziz, M.A., Saleem, M., and Al-Harthi, M.A., 2022. Cellulose Nanocrystals from Office Paper Waste for Green Mortar: Process Optimization Modeling, Characterization, and Mechanical Properties. *Arabian Journal for Science and Engineering*, 47 (4), 5377–5393.